J Mater Sci (2010) 45:4934–4944
DOI 10.1007/s10853-009-4184-2

ICAM 2009

Environmental green chemistry applications of nanoporous carbons

Juan Matos · Andreína García · Po S. Poon

Received: 16 October 2009 / Accepted: 28 December 2009 / Published online: 14 January 2010

Abstract Influence of surface properties of nanoporous carbons on activity and selectivity during the photooxidation of 4-chlorophenol on UV-irradiated TiO_2 was performed. Characterization by infrared spectroscopy, X-ray photoelectronic spectroscopy and X-ray absorption near edge structure spectroscopy confirm the presence of a contact interface between both solids and suggest the coordination of some functional organic groups of the carbon surface, mainly ethers and carboxylic acids, to metallic centre Ti^{+4} in TiO_2. Changes in surface pH of carbons from basic to neutral or acid remarkably increase the production of 4-chlorocathecol by a factor of 22 on TiO_2–Carbon in comparison of TiO_2 alone. A scheme of interaction between TiO_2 and carbon is proposed to the increased photoactivity of TiO_2 and a reaction mechanism for the different intermediate products detected is also proposed. Results showed that TiO_2–Carbon can be used as an alternative photocatalyst for environmental green chemistry and selective organic synthesis applications.

Introduction

The production of petroleum and gas is followed of significant production of polluted water commonly called production water. This waste presents the highest volume in all petroleum exploration and production process and it is composed of a complex mixture of organic and inorganic materials. For example, phenol or halophenols have been found at different amounts as a function of the characteristics of the reservoir and the age of the well and type of oil to be extracted. An interesting alternative in the treatment of these wasted effluents are the advanced oxidation processes, particularly heterogeneous photocatalysis. This technique using titanium dioxide (TiO_2) as photocatalyst has popularity for treatment and purification of water. However, TiO_2 have several operative limitations as low adsorption capabilities, only UV-absorption of the solar spectra, and low selectivity. Several works have showed beneficial cooperative effects between TiO_2 and different carbon forms [1–13]. We have reported synergistic effects between both solids in the photomineralization of phenol, halo-phenols and herbicides [4–6, 12, 13]. Also, an important challenge for industrial organic chemistry consists in developing chemical processes for a clean environment. This is the field of environmental green chemistry [14, 15]. An interesting alternative for green chemistry processes is heterogeneous photocatalysis, principally, because it directly concerns with several of the twelve principles of green chemistry [16]. TiO_2 is a non-toxic and biocompatible material and it is the most efficient photocatalyst that shows high efficiency for the oxidative photodegradation of hazardous aromatic molecules in polluted water and air. Also, it shows a high selectivity in functionalization of light n-alkanes, in selective mild oxidation of gas and liquid hydrocarbons and in selective oxidation of alcohols and hydroxyl-containing molecules [15]. In short, photocatalysis is a promising route for the 21st century organic chemistry [17] where selective photocatalytic conversions will play a major role, offering an alternative green route for the production of organics. However,

J. Matos (✉) · A. García
Engineering of Materials and Nanotechnology Centre, Venezuelan Institute for Scientific Research, I.V.I.C, 20632, Caracas 1020, Venezuela
e-mail: jmatos@ivic.ve

P. S. Poon
Chemistry Centre, Venezuelan Institute for Scientific Research, I.V.I.C, 20632, Caracas 1020, Venezuela

in aqueous phase, TiO_2 has low selectivity because intermediate products of the photooxidation of aromatic molecules commonly are photomineralized. In previous works we have showed [12, 13] that TiO_2 photoactivity is strongly influenced by activated carbon surface properties. The objective of this work is verify the influence of a contact interface between TiO_2 and nanoporous carbons on the photocatalytic activity of TiO_2 in the 4-chlorophenol photodegradation a well-known halo-aromatic molecule commonly found in production waters. In addition, the influence of surface properties of some selected nanoporous carbons on the selectivity of intermediate products formed during the photooxidation of 4CP on UV-irradiated TiO_2 was studied as a possible strategy for high selective green organic synthesis.

Experimental

Materials

High purity 4-chlorophenol (4CP) was purchased from Aldrich. Photocatalyst was TiO_2 P25 from Degussa. Activated carbons (AC) were prepared from sawdust of *Tabebuia Pentaphyla* wood by two methods. Physical activation ($AC_{H\text{-}type}$ or close AC) by gasification under CO_2 flow or by pyrolysis under N_2 flow at temperatures from 450 up to 1000 °C by 1 h [12]. These AC were denoted $AC_{CO_2\text{-}i}$ and $AC_{N_2\text{-}i}$, being i activation temperature. Chemical activation [13] was also performed ($AC_{L\text{-}type}$ or open AC) after impregnation of precursor with different concentrations of $ZnCl_2$, H_3PO_4 and KOH followed by activation under N_2 flow at 450 °C by 1 h. These carbons were denoted as $AC_{ZnCl_2\text{-}i\%}$, $AC_{H_3PO_4\text{-}i\%}$ and $AC_{KOH\text{-}i\%}$ being i% concentration of $ZnCl_2$, H_3PO_4 and KOH, respectively.

Characterization

Characterization of TiO_2 and activated carbons was performed by B.E.T. surface areas (S_{BET}) and surface pH (pH_{PZC}) and reported elsewhere [12, 13]. The full isotherms of N_2 adsorption in the range of 0.03 up to 630 Torr were measured in a Micromeritics ASAP-2010 apparatus. pH_{PZC} were estimated by the drift method [18]. Characterization of some selected TiO_2–AC photocatalysts was also performed by infrared spectroscopy (FTIR), X-ray photoelectronic spectroscopy (XPS) and X-ray absorption near edge structure spectroscopy (XANES). TiO_2–AC photocatalysts were obtained by mixing TiO_2 with the selected AC in 5 mL of water continuously stirred for 80 min. After this, the mixture was filtered and dried at 120 °C, 12 h. Fourier transform Infra-red (FTIR) experiments were made on a spectrophotometer Magna-IR 560 from Nicolet. The powders were mixed with KBr in a 5% (w/w) mixture. The mixed powder was pressed to tablets of 1 cm diameter at 10 tons for 1 min. The transparent tablets were inserted in the apparatus and the spectra were recorded from 4000 to 400 cm^{-1} with a resolution on 5 cm^{-1}. KBr reference spectrum and CO_2 from ambient have been subtracted to every spectrum. Ex-situ XPS was carried out in an ESCALAB 220i-XL spectrometer (VG scientific) equipped with a hemispherical electron analyzer and a double anode Mg–Al non-monochromatic X-ray source. The pressure in the analysis chamber was kept below 10^{-9}Torr. Samples were protected from exposition to the atmosphere by immersion into an ultra-dry hydrocarbon solvent (purified heptanes) while transferring from the reactor to the preparation chamber of the spectrometer. The Ti K-edge XANES spectras at room temperature were recorded in the "fluorescence-yield mode" at the NSLS (Brookhaven National Laboratory) on beamline U7A using a Stern-Heald-Lytle detector with argon as detector gas. All data were normalized to make pre-edge = 0 and post-edge = 1.

Photocatalytic tests

Experimental conditions of photocatalytic tests have been previously reported [12, 13] but are summarized as follow: 50 mg TiO_2 and 10 mg AC were added under stirring in 25 mL at 20 °C of 100 ppm of 4CP and maintained in the dark by 80 min to reach adsorption at equilibrium. This adsorption time before irradiation was selected because in previous works [12, 13] we found that after this time 4CP achieve equilibrium of adsorption on TiO_2–AC photocatalysts. After this time, 4CP concentration remains constant at dark conditions. Batch photoreactor was a cylindrical flask (Pyrex, 60 mL) with a bottom optical window of 3 cm diameter and open to air [5]. Irradiation was provided by a high-pressure mercury lamp and IR was filtered by a circulating-water cell equipped with a 340 nm cut-off filter. Photons flux emitted by light source was determined by Actinometry using Uranyle Oxalate as actinometer and software Logicien Photon version 1.6. Photon flux estimated was 2.9×10^{15} photons cm^{-2} s^{-1}. Disks (0.45 μm) were used to remove particulate matter from aliquots (0.3 mL) before analysis by HPLC with a UV absorbance detector (280 nm). Besides 4CP, hydroquinone (HQ), benzoquinone (BQ) and 4-chlorocatechol (4CT) were detected as the main intermediate products. From kinetic curves of 4CP disappearance as function of irradiation time, apparent first-order rate constants (k_{app}) were obtained as the best kinetic parameter to compare activity of photocatalysts.

Results and discussion

Characterization of AC

Tables 1 and 2 show a summary of S_{BET} and pH_{PZC} of AC. As expected, the higher activation or pyrolysis temperature the higher the pH_{PZC} which indicate the presence of basic functional groups on the surface of AC and a close topology ($AC_{H\text{-}type}$). A similar trend was observed for S_{BET} where an increase of the thermal treatment leads to an increase of the surface areas up to a maximum of 770 $m^2\ g^{-1}$ around 800 °C ($AC_{CO_2\text{-}800}$) and of 590 $m^2\ g^{-1}$ at 900 °C ($AC_{N_2\text{-}900}$) under CO_2 and N_2 flows, respectively. It is important also to note that if wood is heat at higher temperatures than 800 and 900 °C under CO_2 and N_2 flow, respectively, a decrease in S_{BET} was observed. This could be due to excessive gasification by CO_2 or excessive pyrolysis promoted at high temperatures. Concerning to AC prepared by chemical activation, it can be seen from Table 2 that AC prepared with H_3PO_4 showed lower pH_{PZC} values than those AC prepared with $ZnCl_2$. It can be noted from Table 2 that pH_{PZC} of AC prepared with 1%w/w H_3PO_4 is clearly lower than that obtained for the same concentration of $ZnCl_2$ (4.7 against 6.4). This is the due to H_3PO_4 is a strong Brönsted acid while $ZnCl_2$ is a Lewis acid; therefore, the first one should introduce more positive zeta potential, and our case, more acidic groups on AC surface. Also, it must to be note that AC prepared with KOH showed an apparent unexpected behaviour. Thought KOH is a strong Lewis base, Table 2 show that the higher KOH concentration the lower pH_{PZC} of AC. However, this lowering is only from 7.7 down to 6.1 for the increase of KOH concentration from 1 to 65% w/w. This can be explained by the fact that AC prepared with KOH develops an open topology [19, 20] in comparison of $AC_{H\text{-}type}$. On the other hand, it can be seen from Table 2 that the higher the concentration of impregnation compounds the higher S_{BET} areas having a maxima of about 2485, 1987, and 476 $m^2\ g^{-1}$ for $ZnCl_2$ (35% w/w), H_3PO_4 (35% w/w) and KOH (50% w/w), respectively. It is important to note that employing higher concentrations a clear decrease in S_{BET} is observed. This decrease in S_{BET} has been already reported and in the case of KOH [20] have been explained by a high concentration of steam produced during the thermal decomposition of KOH. In this case, activation would proceeds by a gasification reaction at low temperature: $C + H_2O \rightarrow H_2 + CO$, and due to a higher concentration of steam a decrease in S_{BET} is expected because original microporous texture can be consumed by gasification.

Photocatalytic activity

Concerning to photocatalytic activity of TiO_2–AC, Fig. 1a shows an example of the kinetics of disappearance of 4CP under UV-irradiations obtained on some selected photocatalysts. It can be seen in Fig. 1a that direct photolysis is negligible. Also, Fig. 1a shows that AC alone, specifically $AC_{CO_2\text{-}900}$, is not photoactive. This fact was similar for other AC, in concordance with previous results [2, 3]. Kinetics from Fig. 1a indicate that TiO_2–$AC_{CO_2\text{-}900}$ is clearly more efficient that TiO_2 alone requiring only 12 h of irradiation against about 28 h required by TiO_2 to total photodegradation of 4CP. Photodegradation of 4CP on TiO_2 and TiO_2–$AC_{CO_2\text{-}900}$ showed in Fig. 1a follow an

Table 1 BET surface areas (S_{BET}) and surface pH (pH_{PZC}) of $AC_{H\text{-}type}$

System	S_{BET} (m^2/g)	pH_{PZC}[a]	System	S_{BET} (m^2/g)	pH_{PZC}[a]
TiO_2	50 ± 2	6.5	TiO_2–$AC_{N_2\text{-}1000}$	518 ± 17	8.9
TiO_2–$AC_{CO_2\text{-}900}$	548 ± 21	9.1	TiO_2–$AC_{N_2\text{-}900}$	590 ± 17	8.5
TiO_2–$AC_{CO_2\text{-}800}$	770 ± 16	8.5	TiO_2–$AC_{N_2\text{-}800}$	519 ± 15	8.0
TiO_2–$AC_{CO_2\text{-}700}$	570 ± 14	8.0	TiO_2–$AC_{N_2\text{-}700}$	388 ± 13	7.9
TiO_2–$AC_{CO_2\text{-}600}$	426 ± 13	7.2	TiO_2–$AC_{N_2\text{-}600}$	360 ± 12	7.1
TiO_2–$AC_{CO_2\text{-}450}$	352 ± 5	6.3	TiO_2–$AC_{N_2\text{-}450}$	31 ± 5	6.1

[a] pH_{PZC} with less than 5% of SD

Table 2 BET surface areas (S_{BET}) and surface pH (pH_{PZC}) of $AC_{L\text{-}type}$

System	S_{BET} (m^2/g)	pH_{PZC}[a]	System	S_{BET} (m^2/g)	pH_{PZC}[a]	System	S_{BET} (m^2/g)	pH_{PZC}[a]
TiO_2–$AC_{ZnCl_2\ 65\%}$	2001 ± 60	4.5	TiO_2–$AC_{H_3PO_4\ 65\%}$	1569 ± 47	3.1	TiO_2–$AC_{KOH\ 65\%}$	309 ± 15	6.1
TiO_2–$AC_{ZnCl_2\ 35\%}$	2485 ± 75	4.8	TiO_2–$AC_{H_3PO_4\ 35\%}$	1987 ± 60	3.5	TiO_2–$AC_{KOH\ 50\%}$	476 ± 14	6.5
TiO_2–$AC_{ZnCl_2\ 5\%}$	561 ± 17	6.0	TiO_2–$AC_{H_3PO_4\ 5\%}$	414 ± 12	4.0	TiO_2–$AC_{KOH\ 5\%}$	17 ± 1	7.5
TiO_2–$AC_{ZnCl_2\ 1\%}$	30 ± 1	6.4	TiO_2–$AC_{H_3PO_4\ 1\%}$	188 ± 6	4.7	TiO_2–$AC_{KOH\ 1\%}$	5.2 ± 0.2	7.7

[a] pH_{PZC} with less than 5% of SD

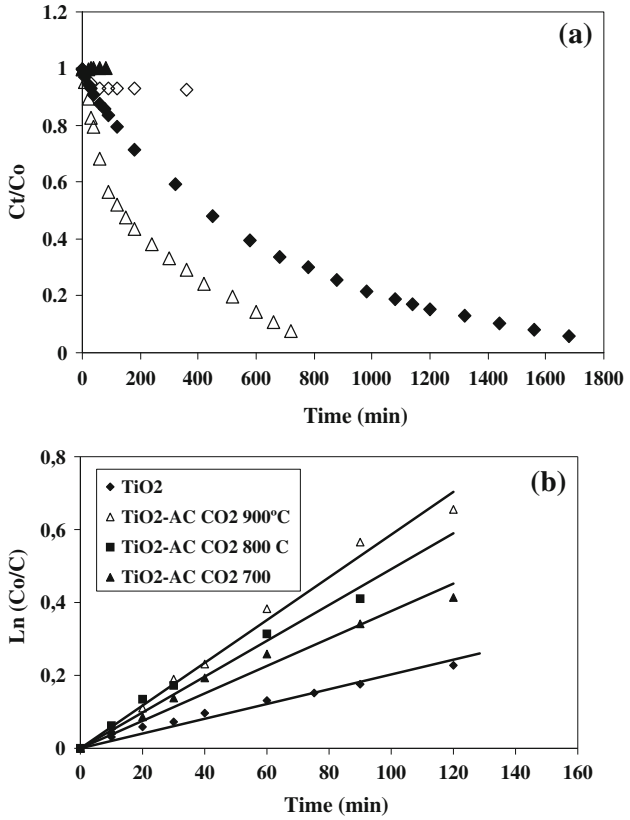

Fig. 1 **a** Kinetics of 4CP disappearance. *filled diamond* TiO_2, *open diamond* Photolysis, *filled triangle* $AC_{CO_2\text{-}900}$, *Open trianlge* TiO_2–$AC_{CO_2\text{-}900}$. **b** Linear regression from kinetic data of some cases in **a**

apparent first order mechanism. Thus, to compare the influence of AC on photoactivity of TiO_2, the first-order apparent constant rate (k_{app}) were obtained from linear regressions $\ln(C_o/C) = k_{app} \cdot (t)$, of kinetic data in Fig. 1a. Figure 1b shows several examples of linear regressions that confirm the apparent first order rate mechanism. Identical treatment of kinetic data was performed for the rest of photocatalyst and a summary of results is presented in Tables 3 and 4 showing the apparent first-order constant (k_{app}) and the interaction factor (I_F) developed between both solids. I_F is defined by comparison between the apparent constant obtained on the mixed system against value obtained on TiO_2 alone:

$$I_F = \left[k_{app}(TiO_2{-}AC_i)/k_{app}(TiO_2)\right]. \quad (1)$$

I_F permits to verify the influence of AC on TiO_2 photoactivity. For example, this parameter indicate that most of TiO_2–AC photocatalysts showed a synergistic effect ($I_F > 1$) between both solids for 4CP degradation and the best mixed system developed a maximum of about three times higher photoactivity than that of TiO_2 alone (Table 3, for TiO_2–$AC_{CO_2\text{-}900}$). We talk about synergy effect if $I_F > 1$ because AC is not photoactive. On the other hand, if $I_F < 1$, there is an inhibiting effect on TiO_2 photoactivity. We attributed these effects to different kind of interactions between TiO_2 and AC. In an early work [2] supported in changes in Langmuir's parameters of phenol adsorption, we reported that this interaction is consequence of a contact interface [2, 4] spontaneously created between both solids. The physicochemical properties of AC, principally surface area (S_{BET}) and surface pH (pH_{PZC}), clearly influences the magnitude of this interface and concomitantly plays an important role on TiO_2 properties, including photoactivity. In general, the higher surface area the higher photoactivity of TiO_2 but this is not the only parameter to be considered because data of Tables 3 and 4 indicate that surface pH plays an important role. For example, in spite that some $AC_{L\text{-type}}$ (Table 2) have remarkably high S_{BET}, as $AC_{ZnCl_2\text{-}65\%}$, $AC_{ZnCl_2\text{-}35\%}$, $AC_{H_3PO_4\text{-}65\%}$, $AC_{H_3PO_4\text{-}35\%}$, contrary to the expected, these AC poorly influence or indeed inhibit Titania photoactivity ($I_F < 1$, Table 4). This inhibition have been ascribed to the fact that pH_{PZC} of those AC are very acidic [13]. Therefore, there is a combination between both physicochemical properties of AC that influence the interaction with TiO_2. The interaction between both solids was confirmed by FTIR, XPS and XANES.

FTIR, XPS, XANES characterization. Interface TiO_2–AC

Figure 2 shows the FTIR spectra of $AC_{CO_2\text{-}900}$, pure TiO_2 and TiO_2–$AC_{CO_2\text{-}900}$. It can be seen that compared with the

Table 3 Summary of kinetics results of 4CP photodegradation of TiO_2–$AC_{H\text{-type}}$

System	$k_{app} \times 10^{-3}$ (min^{-1})	I_F[a]	System	$k_{app} \times 10^{-3}$ (min^{-1})	I_F[a]
TiO_2	2.02	1.00	TiO_2–$AC_{N_2\text{-}1000}$	4.31	2.13
TiO_2–$AC_{CO_2\text{-}900}$	5.85	2.90	TiO_2–$AC_{N_2\text{-}900}$	3.37	1.67
TiO_2–$AC_{CO_2\text{-}800}$	4.91	2.43	TiO_2–$AC_{N_2\text{-}800}$	1.54	0.76
TiO_2–$AC_{CO_2\text{-}700}$	3.78	1.87	TiO_2–$AC_{N_2\text{-}700}$	1.34	0.66
TiO_2–$AC_{CO_2\text{-}600}$	2.29	1.13	TiO_2–$AC_{N_2\text{-}600}$	1.07	0.53
TiO_2–$AC_{CO_2\text{-}450}$	2.16	1.07	TiO_2–$AC_{N_2\text{-}450}$	0.92	0.46

[a] Synergy or inhibition described by $I_F = [k_{app(TiO_2-AC)}/k_{app(TiO_2)} + k_{app(AC\text{-}i)}]$

Table 4 Summary of kinetics results of 4CP photodegradation of TiO_2–$AC_{L\text{-type}}$

System	$k_{app} \times 10^{-3}$ (min^{-1})	I_F[a]	System	$k_{app} \times 10^{-3}$ (min^{-1})	I_F[a]	System	$k_{app} \times 10^{-3}$ (min^{-1})	I_F[a]
TiO_2–$AC_{ZnCl_2\ 65\%}$	1.98	0.98	TiO_2–$AC_{H_3PO_4 65\%}$	1.25	0.62	TiO_2–$AC_{KOH\ 65\%}$	2.61	1.29
TiO_2–$AC_{ZnCl_2\ 35\%}$	2.29	1.13	TiO_2–$AC_{H_3PO_4 35\%}$	2.09	1.03	TiO_2–$AC_{KOH\ 50\%}$	2.90	1.44
TiO_2–$AC_{ZnCl_2\ 5\%}$	4.49	2.22	TiO_2–$AC_{H_3PO_4\ 5\%}$	3.36	1.66	TiO_2–$AC_{KOH\ 5\%}$	0.82	0.41
TiO_2–$AC_{ZnCl_2\ 1\%}$	1.59	0.79	TiO_2–$AC_{H_3PO_4\ 1\%}$	2.01	1.00	TiO_2–$AC_{KOH\ 1\%}$	0.53	0.26

[a] Synergy or inhibition described by $I_F = [k_{app(TiO_2-AC)}/k_{app(TiO_2)} + k_{app(AC\text{-}i)}]$

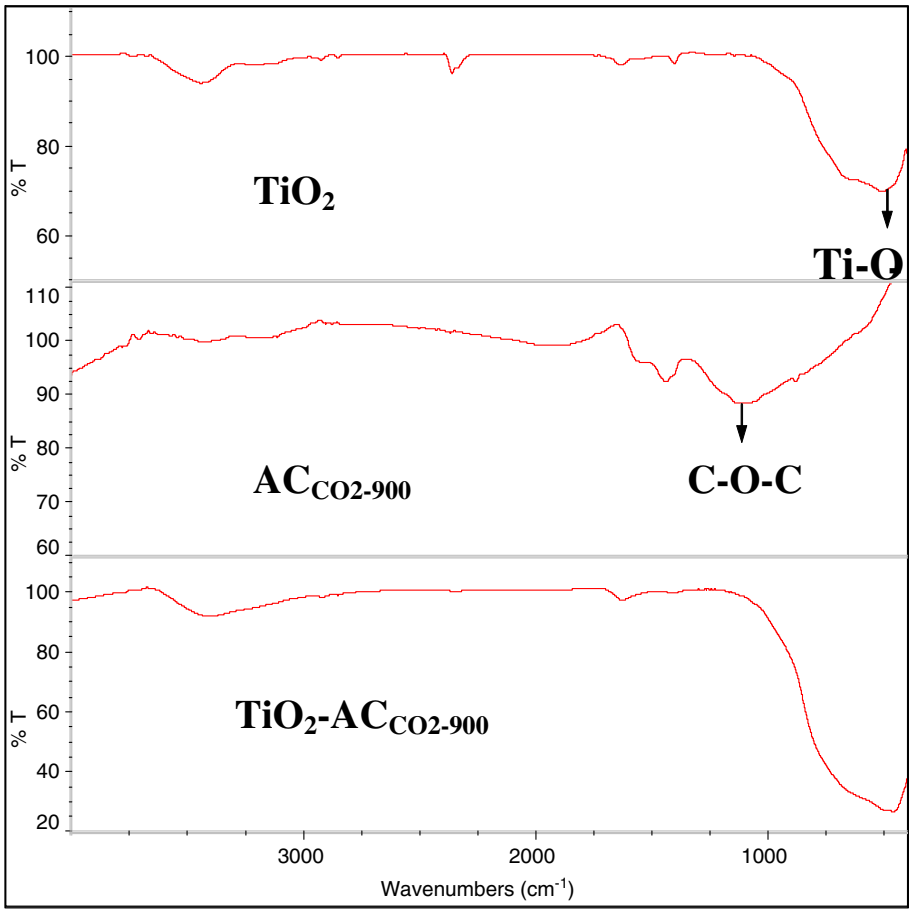

Fig. 2 FTIR of TiO_2, $AC_{CO_2\text{-}900}$ and TiO_2–$AC_{CO_2\text{-}900}$

spectrum of pure TiO_2, a remarkably increase in the stretching absorption band in 500–1000 cm^{-1} of the skeletal O–Ti occur in presence of $AC_{CO_2\text{-}900}$. At the same time, a clear decrease in the cyclic ether (C–O–C) stretching signal of $AC_{CO_2\text{-}900}$) suggest that interaction between both solids would occur by the coordination of oxygenated functional organic groups on AC's surface to TiO_2. Under the effect of oxygen atoms from surface of AC, the symmetry of Ti–O tetrahedron in TiO_2 is broken and therefore, and increase in the absorption band is observed. The influence of functional groups AC on TiO_2 FTIR spectra have been confirmed with other kind of AC. For example, a band corresponding to the stretching of Ti–O–C surface was detected [6] for the case of interaction of TiO_2 with AC. In that work we found that some acidic AC, particularly those with acetate or carboxylate functional groups (for example, $AC_{ZnCl_2\text{-}5\%}$ and $AC_{H_3PO_4\text{-}5\%}$) increased TiO_2 photoactivity as can be seen in the present work in Table 4. Concerning to XPS spectra, it can be seen in Fig. 3 that in presence of AC, a decrease in the binding energy corresponding to Ti 2p signal. This is indicative of reduced Ti states [21] and corresponds to a partial reduction of the oxidation state of Ti from Ti^{+4} to Ti^{+3} of about 1.3 eV when TiO_2 interact with the more basic activated carbon, $AC_{CO_2\text{-}900}$ (9.1 pH_{PZC}) in stead of only 0.5 eV in presence of $AC_{CO_2\text{-}450}$ (6.3 pH_{PZC}). Therefore, it seems clear that pH_{PZC} of AC influence the valence state of Ti in TiO_2–AC. This is in agreeing with previous results [12, 13] where surface aggregation of TiO_2

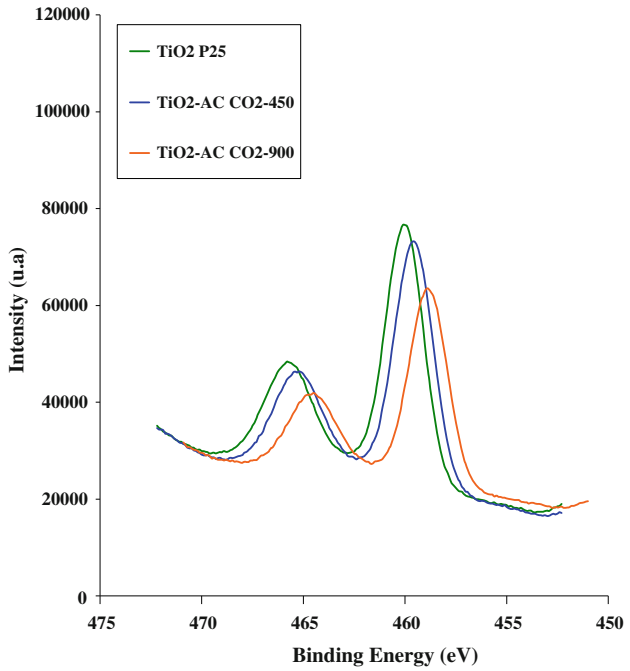

Fig. 3 XPS of TiO_2 and selected TiO_2–AC in the region 2p Ti

nanoparticles on AC was detected by scanning electron microscopy for the case of acid AC [13] while dispersion of TiO_2 was improved in presence of basic AC [12]. This interfacial interaction between both solids was confirmed by XANES studies as follows. Figure 4 shows Ti K-edge XANES spectra for TiO_2 and TiO_2–$AC_{CO_2\text{-}450}$, TiO_2–$AC_{CO_2\text{-}600}$, TiO_2–$AC_{CO_2\text{-}900}$. In Fig. 4 can be seen that changes in the shifts of the Ti K-edge position are minor suggesting that oxidation state of the Ti ions change only a little. However, the three pre-edge features give more information because changes in the pre-edge intensity are associated with reduced Ti states [22]. These changes are highly correlated to the energy position of the Ti K-edge. As observed in the Fig. 4, the larger is the Ti K-edge position, the smaller is the pre-edge intensity. The changes in the pre-edge intensity may be due to the oxygen vacancies produced in the crystal lattice of TiO_2. This is because the 4-(TiO_4), 5-[(Ti = O)O_4] and 6-(TiO_6) coordinated Ti are attributed to the pre-edge peaks between 4969 and 4972 eV [22], commonly assigned 1s-to-3d transitions. The oxidation state of the Ti ions is expected to be higher with fewer amounts of oxygen vacancies inside the crystal lattice. Thus, the intensity changes of the pre-edge feature may be explained by the different amount of oxygen vacancies inside the crystal lattice. Larger amount of oxygen vacancies will produce a more significant pre-edge feature in the XANES spectra. In other words, oxidation state of Ti ions is expected to be lower with more oxygen inside the crystal lattice of TiO_2 as suggested the increase of intensity in the pre-edge of Ti in XANES spectra in Fig. 4. In short, present

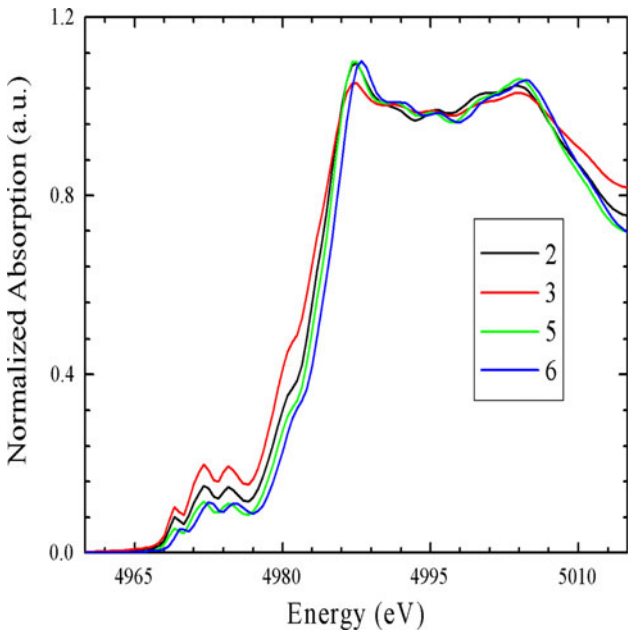

Fig. 4 Ex situ Ti K-edge XANES. (*2*) TiO_2–$AC_{CO_2\text{-}600}$; (*3*) TiO_2–$AC_{CO_2\text{-}900}$; (*5*) TiO_2–$AC_{CO_2\text{-}450}$; (*6*) TiO_2

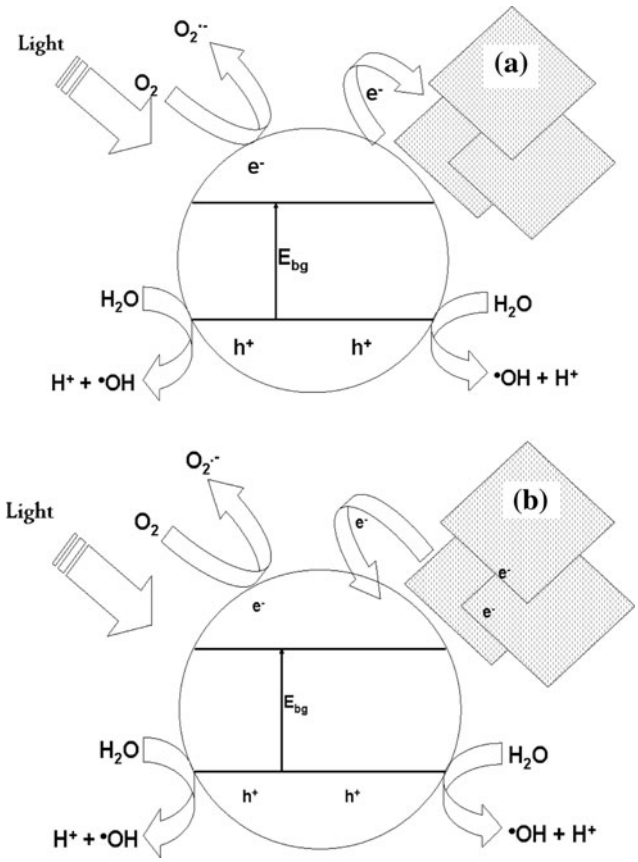

Fig. 5 Interaction mechanism between AC and TiO_2. **a** TiO_2–$AC_{H\text{-}type}$. **b** TiO_2–$AC_{L\text{-}type}$

results suggest that an increase in pH_{PZC} of AC clearly introduces an enhancement in Titania's photoactivity during the 4CP degradation. Figure 5 shows a schematic representation of the interaction between TiO_2 and both types of AC. In the case of TiO_2–$AC_{H\text{-}type}$ (Fig. 5a), activated carbons play the role of electron carrier that could inhibit the recombination of photoelectrons. Figure 5a shows that excited photoelectrons once excited and in conduction band are driven out from TiO_2 surface. This is perfectly logical to think because $AC_{H\text{-}type}$ behaves as an electron semiconductor in totally concordance with a recent study or Peralta et al. [23] whose found that the level of the conduction band of TiO_2 is −0.5 eV versus NHE (normal hydrogen electrode), and the reduction potential of oxygen for the one-electron reduction is −0.2 eV versus NHE. Since this value is less negative than that of the conduction band of TiO_2, the electron transfer from the semiconductor to the carbon particle is thermodynamically favored. On the other side, Fig. 5b shows the contrary behaviour. Photoelectrons can be added to TiO_2 surface because $AC_{L\text{-}type}$ have specific functional organic groups that in solution are dissociated to produce surface anions able to drive out electron density from aromatic system to TiO_2. This is in agreeing with works from other groups [24, 25] that show that the addition of low concentrations of organic acids as ascorbic [24] or acetic [25] to aqueous suspensions with TiO_2 introduce important modifications to the surface of the semiconductor. Therefore, if the surface concentration of such groups on AC is enough low, which is perfectly valid to consider in the present case because AC prepared at low impregnation concentrations of acids showed the best photocatalytic results, for example TiO_2–$AC_{ZnCl_2\text{-}5\%}$ and TiO_2–$AC_{H_3PO_4\text{-}5\%}$ (Table 4), then, it can be suggested that we are in presence of a similar behaviour than those studies [24, 25]. In other words, for the case of the mixed system TiO_2–$AC_{L\text{-}type}$, the synergy effect detected could be attributed not only to a proper surface area but also to the presence of low surface concentration of acidic oxygenated groups, particularly carboxylic acids. The analogy is perfectly valid because once dissociated in aqueous phase, the carboxylic acid produce carboxyl anions ($–COO^-$) clearly stabilized by transfer electrons to the aromatic ring of graphene layers in AC. Having this in mind, Fig. 6 shows a general mechanism for the degradation of 4CP involving

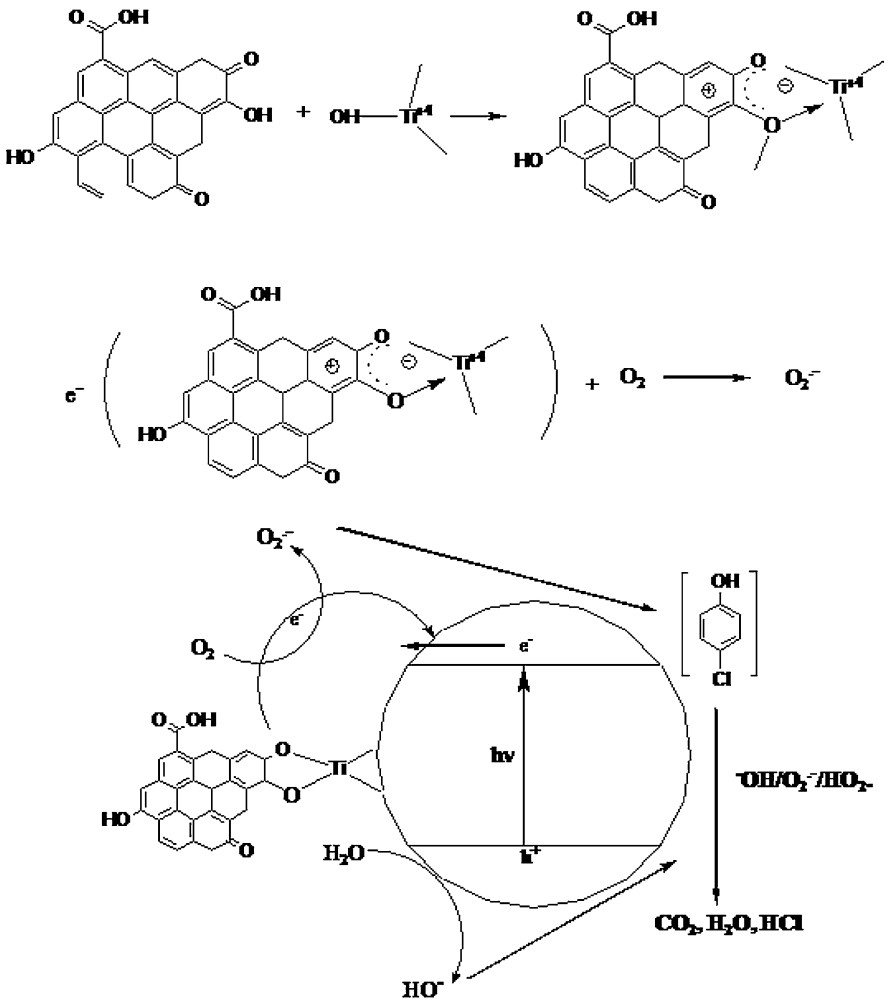

Fig. 6 Mechanism of 4CP degradation on TiO_2–$AC_{L\text{-}type}$

the interaction between both solids. In a first step, it can be seen in Fig. 6 that after dissociation in aqueous phase, carboxylic or acetic acid as functional groups on AC's surface coordinated to Ti^{+4} metallic centre of TiO_2. As described above, this interaction could inhibit the recombination of photogenerated species in the semiconductor (e−, h+). In consequence, a higher concentration of hydroxyl radical ($^{\bullet}OH$) and superoxide anion radical ($O_2^{\bullet-}$) can be formed as indicate the second step of mechanism in Fig. 6. Then the third step shows once adsorbed 4CP, it suffer degradation with $^{\bullet}OH$ and/or $O_2^{\bullet-}$. The influence of $O_2^{\bullet-}$ anion radical is very important because the higher concentration of $O_2^{\bullet-}$ the higher the production of $HO_2^{\bullet}$ radicals that enhance the photoactivity of TiO_2 in the photomineralization of 4CP as indicated third step in mechanism of Fig. 5.

Photoselectivity. Kinetics of appearance and disappearance of intermediate products

According to the type of carbon materials employed, the proportion of the intermediate 4-chlorocatechol detected is clearly increased. This fact can be clearly seen from Fig. 7 that shows the kinetic trends corresponding to the sum of HQ + BQ (Fig. 7a) and 4CT (Fig. 7b). In general, it can be seen from Fig. 7 that for TiO_2 alone and most of TiO_2–$AC_{H_3PO_4}$ photocatalysts, the main intermediate products are HQ + BQ (Fig. 7a). This figure shows that the more acid is the AC employed the higher is the production of intermediate products. Figure 7b clearly shows that the CT formation is clearly higher in the most acid TiO_2–$AC_{H_3PO_4}$ (65, 35, 5% w/w) photocatalysts and practically negligible for the TiO_2–$AC_{H_3PO_4\text{-}1\%}$ and TiO_2 alone. This fact indicates that different surface sites governed by pH_{PZC} more than by texture characteristics leads to different types of 4CP adsorption mechanism and therefore influence the intermediate product distributions. These results are discussed as follow. Intermediate products detected agree with chlorine substitution by p-hydroxylation yielding HQ and BQ that are commonly in equilibrium and to o-hydroxylation yielding 4CT. This general trend was also observed for TiO_2–AC_{N_2} and therefore, Table 5 shows a summary of changes detected in orto/para products in the 4CP photooxidation. R(o/p) compares the maximum quantity detected of 4CT against maxima of HQ and BQ. Values in Table 5 indicate a clear increase of R(o/p) in comparison of that obtained on TiO_2 alone (0.08). R(o/p) yield a maxima value of about 7.453 for TiO_2–$AC_{N_2\text{-}450}$ (pH_{PZC} 6.05). A similar trend was detected for relation F(o/o) that compares the maxima quantity of 4CT detected on TiO_2–AC against maxima 4CT on TiO_2 (0.037 μmol). It can be seen from Table 5 that for the case of $AC_{N_2\text{-}700}$ against $AC_{N_2\text{-}1000}$ a change in only one unity of surface pH (from 8.9 to 7.9) leads to a remarkably increase in F(o/o) from 1.60 up to a maxima of about 22.1 for TiO_2–$AC_{N_2\text{-}700}$. A similar behaviour is detected for the other type of AC which is clearly more acid than those prepared by pyrolysis. In addition, having in mind that 4CP photooxidation

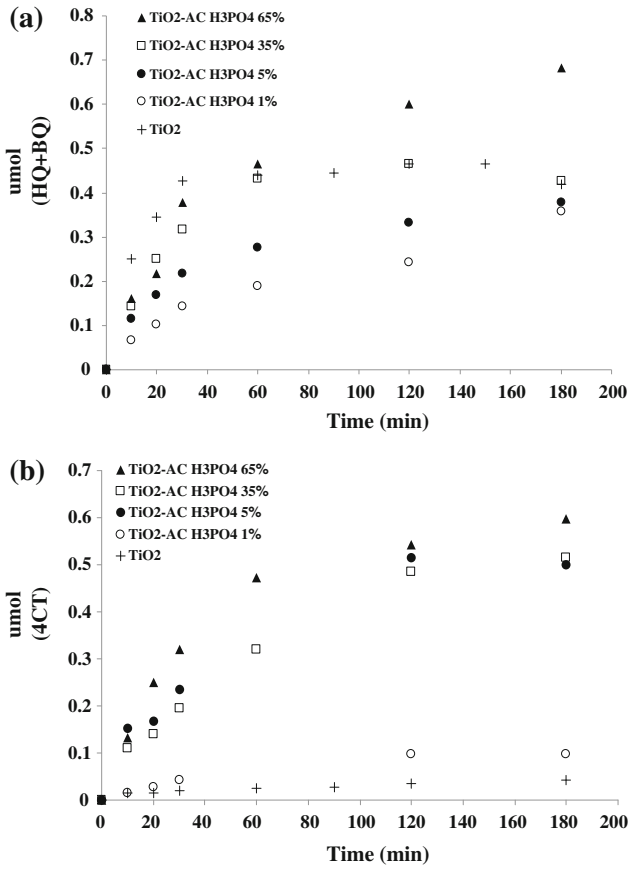

Fig. 7 Kinetics of appearance and disappearance of main intermediates products in 4CP photooxidation in presence of $AC_{H_3PO_4}$ **a** HQ + BQ. **b** 4CT

Table 5 Intermediate products in the photooxidation of 4CP on TiO_2–AC

Photocatalyst	HQ + BQ (μmol)	4CT (μmol)	R (o/p)	F (o/o)
TiO_2	0.476	0.037	0.08	1.00
TiO_2–$AC_{N_2\text{-}1000}$	0.487	0.059	0.12	1.60
TiO_2–$AC_{N_2\text{-}900}$	0.300	0.068	0.23	1.84
TiO_2–$AC_{N_2\text{-}800}$	0.210	0.680	3.24	18.4
TiO_2–$AC_{N_2\text{-}700}$	0.139	0.817	5.88	22.1
TiO_2–$AC_{N_2\text{-}600}$	0.135	0.805	5.96	21.8
TiO_2–$AC_{N_2\text{-}450}$	0.106	0.790	7.45	21.4
TiO_2–$AC_{H_3PO_4\text{-}1\%}$	0.363	0.108	0.30	2.92
TiO_2–$AC_{H_3PO_4\text{-}5\%}$	0.381	0.493	1.29	13.3
TiO_2–$AC_{H_3PO_4\text{-}35\%}$	0.442	0.540	1.22	14.6
TiO_2–$AC_{H_3PO_4\text{-}65\%}$	0.690	0.642	0.93	17.4

occurs on TiO_2 surface, the present results clearly showed that light changes in pH_{PZC} of AC induce important changes in the surface of semiconductor and this clearly affect the reaction mechanism. Figure 8 shows the influence of pH_{PZC} of the different carbons, AC_{N_2} (Fig. 8a) and $AC_{H_3PO_4}$ (Fig. 8b). It can be seen in Fig. 8 that the lower the pH_{PZC} of AC the higher the values of *R* and *F* indicated in Table 5. In the photooxidation of 4CP there are two possible reaction mechanisms. First, the oxidation of 4CP can occur by nucleophilic substitution of chlorine by the attack of aromatic ring with $^{\bullet}OH$ radicals that are promoted at neutral or basic pH. This route yield preferentially HQ and its successive oxidation yield BQ. On the other hand, the oxidation of 4CP would occur by oxidation of aromatic ring by electrophilic addition of anion radical $O_2^{\bullet-}$ yielding selectivity 4CT. This mechanism is favored at acid pH.

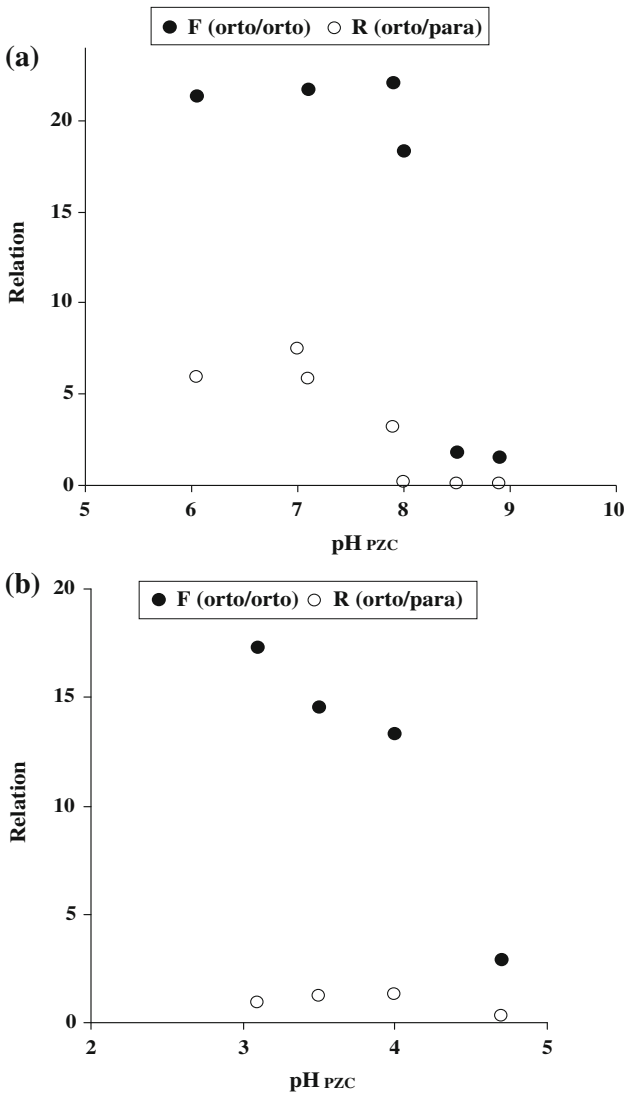

Fig. 8 Influence of pH_{PZC} of activated carbon on selectivity. **a** AC_{N_2}, **b** $AC_{H_3PO_4}$

These results are in totally concordance with previous studies concerning to photooxidation of phenol [2] and 2,4-dichlorophenoxiacetic acid [5]. These remarkably differences in products selectivity as function of AC's pH_{PZC} can be associated with interfacial interaction detected between both solids discussed above. For example, for the case of the transfer of electrons from Titania to AC (Fig. 5a), this kind of interaction permits to increase $^{\bullet}OH$ radicals in agreeing with the strong oxidation of 4CP by means of a mechanism to mainly produce para-products (Table 5) as hydroquinone (HQ) and benzoquinone (BQ). This p-hydroxylation mechanism is showed in Fig. 9. This mechanism is induced by basic surface pH of AC and it involves the abstraction of a hydride and chloride from 4CP to produce bencine (structure 2A) which is readily oxidized to produce HQ, commonly in equilibrium with BQ. On the other hand, the interaction between TiO_2 and AC by the way showed in Fig. 5b, promotes higher concentrations of $O_2^{\bullet-}$ and $HO_2^{\bullet}$ (obtained from $O_2^{\bullet-} + H^+$) radicals whose induce remarkable changes in selectivity of products (Table 5) to mainly produce orto-product (Table 5) as 4-chlorocathecol (4CT). This o-hydroxylation mechanism is showed in Fig. 10. It is induced by acid surface pH of AC and involves the abstraction of an electron from 4CP to produce an aromatic cation radical (structure 6A) which is stabilized by resonance to produce the structure 6C (Fig. 10) which is readily oxidized to produce selectively 4CT and H_2O_2, a common sub-product obtained in the present experimental conditions. According to this, the interpretation of pH effects on the selective photooxidation of 4-chlorophenol is a very difficult task because the pH of the solution influences adsorption and dissociation of substrate, catalyst surface charge, oxidation potential of the valence band and other physicochemical properties of the system. In reality, the interpretation of pH effects on the selective photooxidation of 4-chlorophenol is a very difficult task because the pH of a solution influences adsorption and dissociation of substrate, catalyst surface charge, oxidation potential of the valence band and other physicochemical properties of the system. Therefore, we are working on characterization of TiO_2–AC composites by surface techniques as X-ray photoelectronic spectroscopy, and electron and photoelectronic conductivity to better elucidate the effect of TiO_2–AC for the selective photooxidation of 4-chlorophenol a little more deeply.

Finally, it must to be remark that nowadays a challenge for the heterogeneous photocatalysis consists in improving the photocatalytic efficiency of TiO_2 by shifting its optical response to the visible range [10]. One of the most interesting ways to modify this semiconductor to absorb visible light consists in doping with transition metals and other elements. For example, several attends have been performed by doping with iron [9], carbon [10] and more recently, the

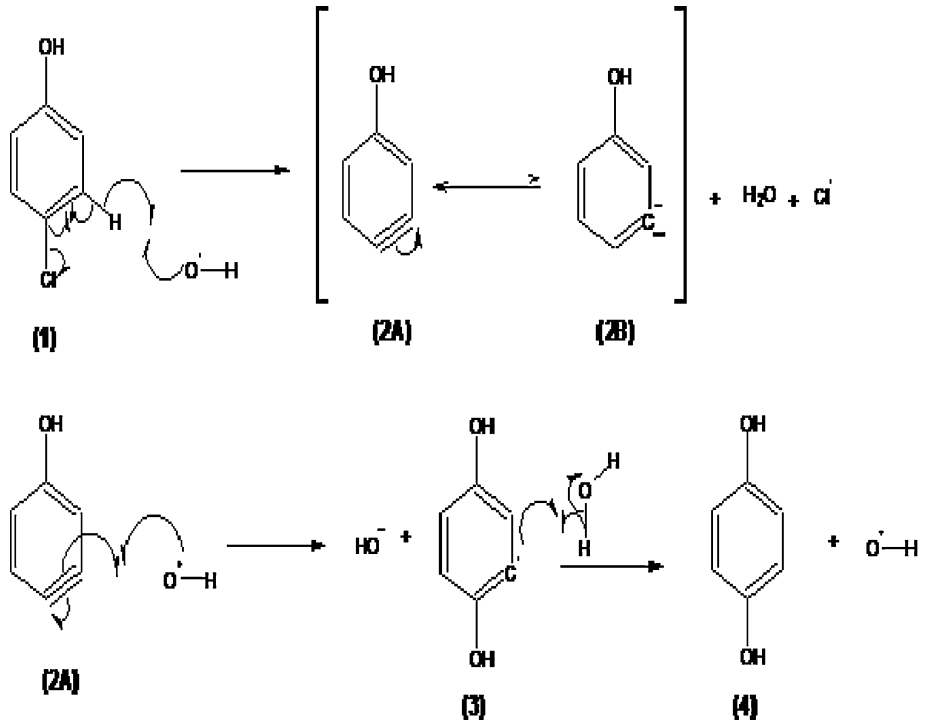

Fig. 9 para-Hydroxylation mechanism induced by basic surface pH and close topology of AC

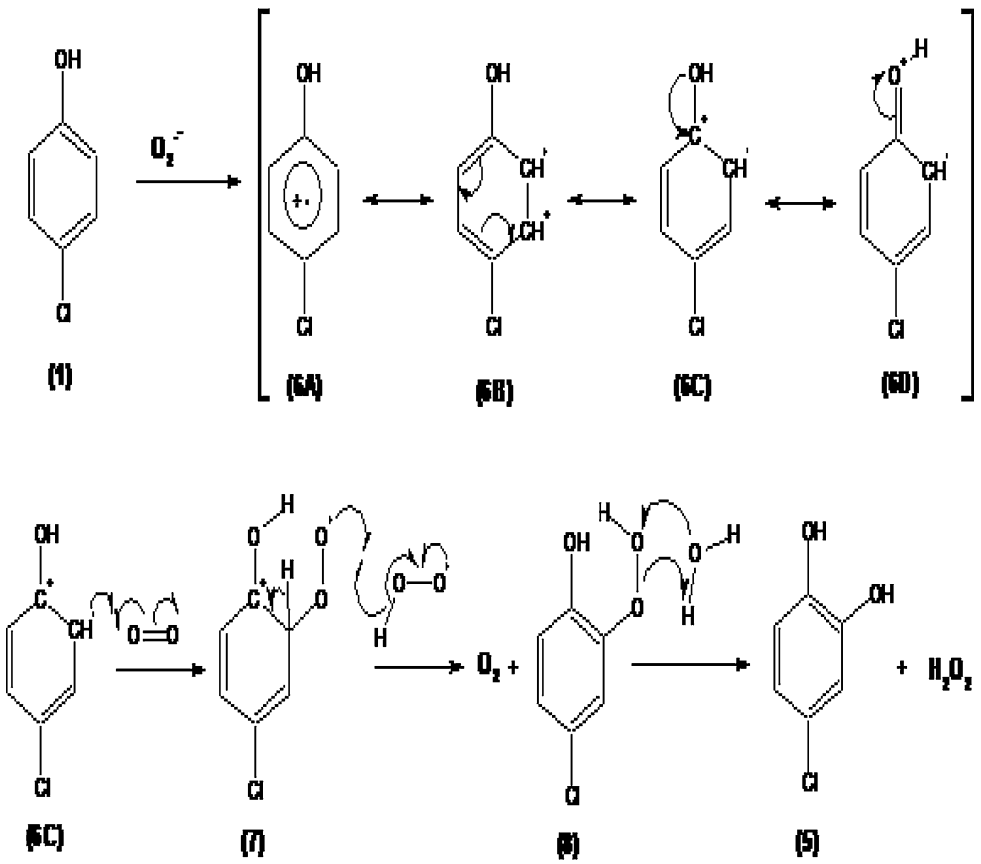

Fig. 10 ortho-Hydroxylation mechanism induced by acid surface pH and open topology of AC

effect of rare-earths [26] and nitrogen [27, 28] as TiO_2–doping elements have been studied for the degradation of dyes and azo-dyes and results obtained have been promising ones. Regarding our own experience, we are studying TiO_2–doped photocatalysts with Fe, N, P and C for tune the process for visible range and up to now the best results (preliminary ones) have been obtained with C and P as doping elements.

Conclusions

FTIR, XPS and XANES characterization of TiO_2–AC suggest a strong interaction between TiO_2 and AC and from these evidences, a mechanism for the interaction between both solids was proposed. This mechanism explains both the improved photoactivity of TiO_2 as a function of the surface pH of different types of activated carbon and changes in products distributions. The design of pH_{PZC} of AC permits the control in the selectivity of products during 4CP photooxidation on TiO_2–AC. Results suggest the possibility to use TiO_2–AC as an alternative environmental green photocatalyst both in treatments of wasted waters and in selective organic synthesis.

Acknowledgements Authors would like to thanks to NSLS, Chemistry Department of Brookhaven National Laboratory for XANES analysis.

References

1. Torimoto T, Okawa Y, Takeda N, Yoneyama H (1997) J Photochem Photobiol A: Chem 103:153
2. Matos J, Laine J, Herrmann JM (1998) Appl Catal B: Environ 18:281
3. Matos J, Laine J, Herrmann JM (1999) Carbon 37:1870
4. Herrmann JM, Matos J, Disdier J, Guillard C, Laine J, Malato S, Blanco J (1999) Catal Today 54:255
5. Matos J, Laine J, Herrmann JM (2001) J Catal 200:10
6. Matos J, Laine J, Herrmann JM, Uzcategui D, Brito JL (2007) Appl Catal B: Environ 70:461
7. Araña J, Rodriguez JM, Tello E, Garriga C, Gonzalez O, Herrera JA et al (2003) Appl Catal B: Environ 44:161
8. Araña J, Rodriguez JM, Tello E, Garriga C, Gonzalez O, Herrera JA et al (2003) Appl Catal B: Environ 44:153
9. Tryba B, Morawski AW, Inagaki M, Toyoda M (2006) Appl Catal B: Environ 63:215
10. Ren W, Ai Z, Jia F, Zhang L, Fan X, Zou Z (2007) Appl Catal B: Environ 69:138
11. Wang W, Gomez Silva C, Faria JL (2007) Appl Catal B: Environ 70:470
12. Cordero T, Duchamp C, Chovelon JM, Ferronato C, Matos J (2007) Appl Catal B: Environ 73:227
13. Cordero T, Duchamp C, Chovelon JM, Ferronato C, Matos J (2007) J Photochem Photobiol A:Chem 191:122
14. Anpo M (2000) Pure Appl Chem 72:1265
15. Herrmann JM, Duchamp C, Karkmaz M, Hoai BT, Lachheb H, Puzenat E, Guillar C (2007) J Hazard Mater 146:624
16. Anastas PT, Warner JC (1998) Green chemistry: theory and practice. Oxford University Press, New York
17. Palmisano G, Augugliaro V, Pagliaro M, Palmisano L (2007) Chem Comm 33:3425
18. Lopez MV, Stoeckli F, Moreno C, Carrasco F (1999) Carbon 37:1215
19. Matos J, Labady M, Albornoz A, Laine J, Brito JL (2004) J Mater Sci 39:3705. doi:10.1023/B:JMSC.0000030724.32255.b0
20. Matos J, Labady M, Albornoz A, Laine J, Brito JL (2005) J Mol Catal A: Chem 228:189
21. Kim S, Lim SY (2008) Appl Catal B: Environ 84:16
22. Hsiung TL, Wang HP, Wang HC (2006) Radiat Phys Chem 75:2042
23. Peralta JM, Manríquez J, Meas Y, Rodríguez FJ, Chapman TW, Maldonado MI et al (2007) J Hazard Mater 147:588
24. Ou Y, Lin JD, Zou HM, Liao DW (2005) J Mol Catal A: Chem 241:59
25. Araña J, Doña JM, González O, Herrera JA, Fernández C, Pérez J (2006) Appl Catal A: General 129:274
26. Du P, Bueno-López A, Verbaas M, Almeida AR, Makke M, Moulijn JA, Mul G (2008) J Catal 260:75
27. Yu C, Yu JC (2009) Catal Lett 129:462
28. Wang Y, Zhou G, Li T, Qiao W, Li Y (2009) Catal Commun 10:412